ONLINE PUBLICATION DATE:

Original Research

Cr (VI) Removal by Polyethyleneimine and Magnetically Modified Garden Waste Biochar

Jingxi Tie[1], Yang Shao[1], Mengjia Yan[1], Xiaohan Duan[1,2]*

[1]School of Environmental and Municipal Engineering, North China University of Water Resources and Electric Power, Zhengzhou, 450045, PR China
[2]Henan Vocational College of Water Conservancy and Environment, Zhengzhou 450008, PR China

Abstract

In this study, garden waste, polyethyleneimine, and Fe^{2+}/Fe^{3+} were used as starting materials to create polyethyleneimine and magnetically modified biochar derived from garden waste ($P/Fe_3O_4@GWBC$). The best condition for the preparation of the composite was explored in order to produce $P/Fe_3O_4@$ GWBC for batch testing on Cr (VI) removal. $P/Fe_3O_4@GWBC$ had a rough surface with numerous fine particles, which was a typical composite with both micropore and mesopore. The experiment's findings indicated that the acid environment was favorable for Cr (VI) adsorption. The adsorption process could be properly described by the pseudo-second-order kinetics model. The isotherm investigation demonstrated the monolayer adsorption of Cr (VI) by the appropriate fitting utilizing the Langmuir equation. The highest Cr (VI) uptake computed using the Langmuir equation was 52.6 mg/g, ranking fourth among 11 composites. The investigation of thermodynamics revealed that the adsorption process was spontaneous and endothermic. The main mechanisms for Cr (VI) removal include electrostatic adsorption, ion exchange, chelation, and Cr (VI) reduction.

Introduction

Chromium is a common heavy metal that is released by a number of industries. In the environment, it mostly takes the forms of trivalent chromium (Cr (III)) and hexavalent chromium (Cr (VI)) [1, 2]. Even at extremely low concentrations, Cr (VI) may seriously harm aquatic life and water consumers. Additionally, it is far more hazardous than Cr (III) [1, 3, 4]. As a result, Cr (VI) needs to be polished before the Cr (VI)-bearing wastewater is discharged into the water bodies.

Adsorption has been demonstrated by other researchers, and in our earlier work, to be an effective method for the elimination of Cr (VI) [5-7]. Due to its many advantages, such as its affordability, ease of manufacture, environmental friendliness, adaptability, high stability, and abundant supply of raw materials, biochar (BC) has been widely used as an adsorbent for adsorption removal of a variety of pollutants [8-12]. Agricultural waste mainly includes plant waste, agricultural and sideline products processing waste, and so on [13-15], which has a loose, porous structure and contains carboxyl, hydroxyl, and other reactive

---

*e-mail: 15202843@qq.com
Tel.: +86-37-165-790-528

groups to be used as a biomass adsorption material in the field of pollution control [16]. At present, a great deal of research has been done on taking advantage of agricultural wastes as biomass adsorbents for the treatment of pollutants, such as organic pollutants and heavy metals pollutants [17-21].

However, biochar has to be modified for Cr (VI) adsorption due to a lack of active sites in its pristine state [22, 23]. The efficacy of chemicals rich in amino groups, such as polypyrrole, polyaniline, polyethyleneimine, chitosan, and others, has been demonstrated by their amine and imine groups' ability to remove Cr (VI) through electrostatic adsorption and chelation [7, 24, 25]. In addition, their advantages, such as easy synthesis, robust ion exchange capacity, and environmental stability, account for their widespread use in biochar modification [24].

Polyethyleneimine (PEI) has been shown in our earlier work to be useful in enhancing Cr (VI) adsorption by biochar made from garden waste. However, because of its comparable density to the solution, the composite is challenging to separate after adsorption.

Fe^{2+}/Fe^{3+} coprecipitation and PEI modification were employed in this study to improve the biochar's ability to remove Cr (VI) and make it easier to separate from the solution. The conversion of Cr (VI) into Cr (III) further improved Cr (VI) removal [7, 26]. The best conditions for the manufacture of the composite were explored. Batch Cr (VI) adsorption tests were conducted to explore its Cr (VI) adsorption ability and Cr (VI) removal mechanism.

Materials and Methods

Adsorbent Preparation

Garden waste (GW) was collected from the North China University of Water Resources and Electric Power, Zhengzhou, China. GW was dried and sieved using 0.15 mm mesh. 15 g of GW powder was calcined at 800°C in a tube furnace for 4 h, which was determined in our previous study to be the best condition for GWBC preparation in the N_2 atmosphere.

The Fe^{2+}/Fe^{3+} coprecipitation adopted in the previous research was used to prepare the magnetic GWBC (Fe_3O_4@GWBC). Briefly, Fe_3O_4@GWBC was prepared by adding GWBC, $FeCl_3 \cdot 6H_2O$, $FeSO_4 \cdot 7H_2O$ at different ratios into 200 ml deionized water (W:W:W= 0.1:1.0:0.56, 0.5:1.0:0.56, 1.0:1.0:0.56, 1.5:1.0:0.56 and 2.0:1.0:0.56) since $FeCl_3 \cdot 6H_2O$: $FeSO_4 \cdot 7H_2O$=1.0:0.56 was used for Fe_3O_4 preparation determined in previous study [27]. Therefore Fe_3O_4@GWBC was made by adding GWBC, $FeCl_3 \cdot 6H2O$, and $FeSO_4 \cdot 7H_2O$ at varied ratios into 200 ml deionized water (W:W:W= 0.1:1.0:0.56, 0.5:1.0:0.56, 1.0:1.0:0.56, 1.5:1.0:0.56 and 2.0:1.0:0.56). The adsorbents that were made using distinct ingredients were identified by their labels, which were Fe_3O_4@GWBC1, Fe_3O_4@GWBC2, Fe_3O_4@GWBC3, Fe_3O_4@

GWBC4 and Fe_3O_4@GWBC5. 1% NaOH was added dropwise into the mixture, being stirred at 150 rpm and 90°C until its pH rose to 11 in a water bath. The mixture was stirred for another 1 h for a complete reaction. After gathering the black precipitate, deionized water was used to wash it until the pH was stable. To get the magnetic GWBC, the black particles were crushed and dried in a vacuum at 50°C before being passed through a 0.15 mm sieve once more.

1g Fe_3O_4@GWBC was dispersed into 20 ml 10% (mass fraction) PEI-methanol solution combination and stirred at 160 rpm and 30°C for 5 h. The mixture was stirred for another 30 minutes and filtered after 40 ml 1% (mass fraction) glutaraldehyde solution was added. The solid was dried in an oven at 65°C after being washed using deionized water to get the final adsorbent (P/Fe_3O_4@GWBC).

GWBC was first modified using PEI and by Fe^{2+}/Fe^{3+} coprecipitation in sequence using the same parameter mentioned above to get Fe_3O_4@PGWBC.

Adsorbent Characterization

An automatic specific surface area analyzer (Belsorp-max, Japan) was used to determine the BET-specific surface area and the total BJH pore volume and pore size distribution. The surface morphology of samples was observed by scanning electron microscopy (SEM, Zeiss Genimi500, Germany). The chemical states of the atoms in the samples were investigated by X-ray photoelectron spectroscopy spectrometer (XPS, Escalab 250Xi+, USA). A Fourier transform infrared spectroscopy (FTIR, Nicolet IS50, USA) was used to analyze the functional groups of the samples. The X-ray diffraction spectra of the samples were recorded using a diffractometry machine (XRD, ZSX Primus II, Japan). The zeta potential of the sample was determined using a zeta potential meter (Particle Metrix GmbH, Germany).

Batch Adsorption Experiment

Static adsorption experiments were carried out to explore the Cr (VI) removal performance of the prepared adsorbent in the following way: 20 mg of adsorbent was put into 50 mL Cr (VI)-containing wastewater, and the mixture was shaken at 120 rpm for various temperatures and times. The residual Cr (VI) in the filtrates was examined by a UV-vis spectrophotometer (UV-5100, Yuanxi, China) using the 1,5-diphenylcarbazide method at 540 nm. All the experiments were done in triplicate.

Results and Discussion

Determination of the Optimal Condition for Adsorbent Preparation

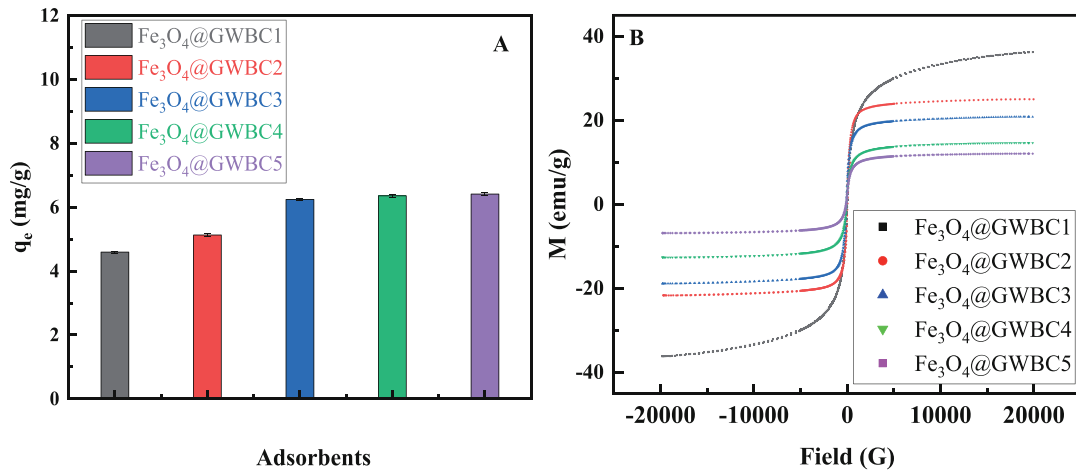As shown in Fig. 1A, Cr (VI) adsorption of five Fe_3O_4@GWBCs increased significantly with the rising

Fig. 1. Cr (VI) adsorption and VSM diagrams of Fe_3O_4@GWBC prepared at different raw material ratios (T=298 K, t=4 h).
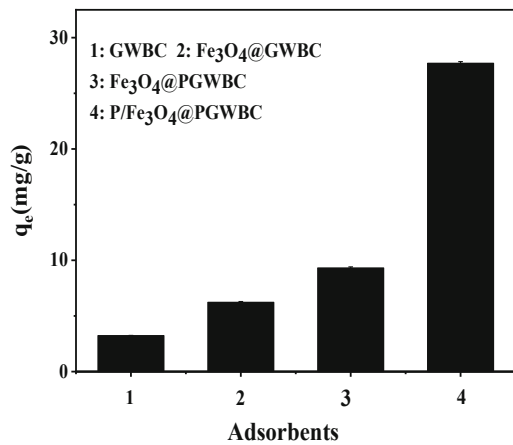
Fig. 2. Cr (VI) adsorption by GWBC, Fe_3O_4@GWBC, Fe_3O_4@PGWBC, and P/Fe_3O_4@GWBC (T=298 K, t=4 h).

(Fig. 1B). As a result, 1g GWBC, namely, GWBC:FeCl$_3$·6H$_2$O:FeSO$_4$·7H$_2$O=1.0:1.0:0.56 was determined to be the best formula for Fe_3O_4@GWBC preparation, taking into account both its Cr (VI) adsorption and magnetic separation.

Fig. 2 shows the Cr (VI) adsorption using GWBC, Fe_3O_4@GWBC, Fe_3O_4@PGWBC, and P/Fe_3O_4@GWBC. P/Fe_3O_4@GWBC showed the highest Cr (VI) adsorption of 27.7 mg/g among the four adsorbents, indicating GWBC modified by magnetization and PEI may improve its Cr (VI) adsorption. The modification sequence also considerably impacted the Cr (VI) adsorption. Compared to Fe_3O_4@PGWBC, P/Fe_3O_4@GWBC was superior for Cr(VI) removal because PEI modification after magnetization provided reactive amino groups on its surface. However, magnetization after PEI modification covered the amino groups with Fe_3O_4 particles, which weakened the Cr (VI) adsorption. As a result, P/Fe_3O_4@GWBC was used to carry out the following tests.

As shown in Fig. 3A, GWBC had a relatively smooth surface with a flaky structure, whereas P/Fe_3O_4@

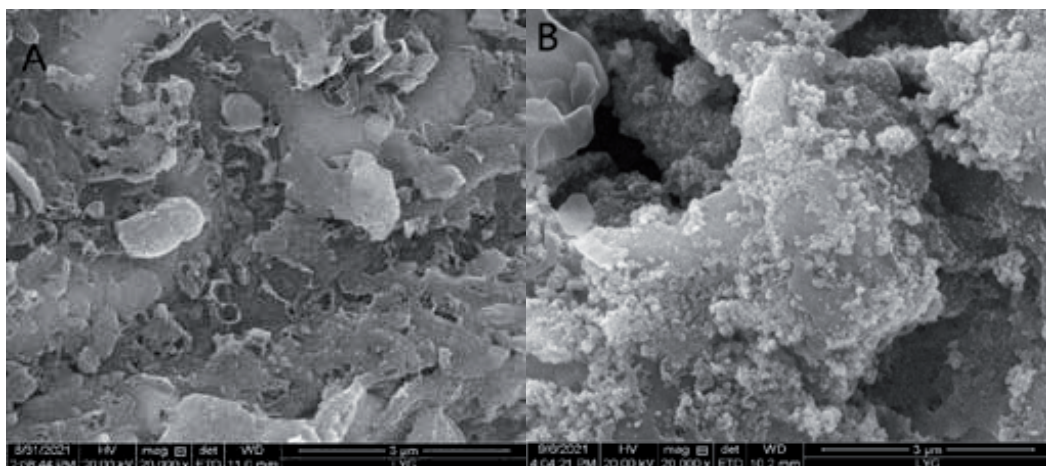GWBC dosage from 0.1 g to 1 g, and further increase of GWBC dosage to 2 g led to faint enhancement of Cr (VI) adsorption, while, the magnetization of Fe_3O_4@GWBCs decreased from 36.23 emu/g to 24.99 emu/g

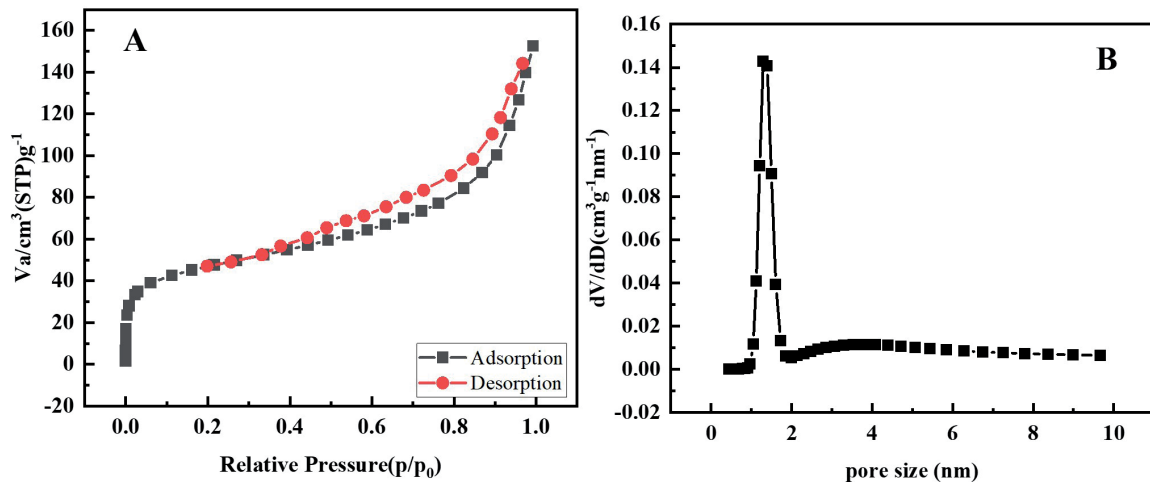Fig. 3. SEM morphologies of GWBC(A) and P/Fe_3O_4@GWBC(B).

Fig. 4. Nitrogen adsorption-desorption isotherms (A) and pore size distribution (B) of P/Fe$_3$O$_4$@GWBC.

Table 1. Specific surface areas and pore textures of P/Fe$_3$O$_4$@GWBC.

Sample	SBET (m^2/g)	Vtot (cm^3/g)	Average pore diameter (nm)
P/Fe$_3$O$_4$@GWBC	165.43	0.23	5.62

GWBC had a rough surface (Fig. 3B) with numerous fine particles on it due to the sequential alteration by magnetization and PEI.

As shown in Fig. 4A, P/Fe$_3$O$_4$@GWBC had type IV N$_2$ adsorption-desorption isotherms with type H4 hysteresis loop, and its S$_{BET}$, V$_{tot}$, and average pore diameter were 165.43 m^2/g, 0.23 cm^3/g and 5.62 nm (Fig. 4B, Table 1), respectively, indicating the composite was a typical composite with both micropore and mesopore.

The structures and crystallinities of GWBC and P/Fe$_3$O$_4$@GWBC was investigated using XRD, and the findings were shown in Fig. 5. The main characteristic peaks at 2θ = 30.17°, 35.52°, 43.17°, 53.58°, 57.24° and 62.69° corresponded to the (220), (311), (400), (422), (511) and (440) planes of Fe$_3$O$_4$ [28-31]. Hence, Fe$_3$O$_4$ was loaded successfully on the P/Fe$_3$O$_4$@GWBC, allowing
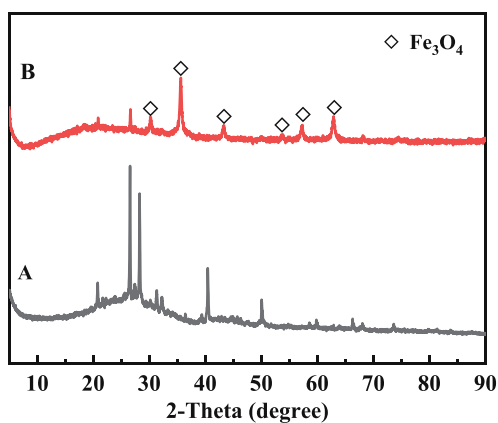
the spent adsorbent to be readily separated from an aqueous solution following adsorption in a magnetic field.

Static Adsorption

As shown in Fig. 6A and 6B, Cr (VI) adsorption by P/Fe$_3$O$_4$@GWBC declined from 37.6 mg/g to 2.2 mg/g as the solution pH increased from 2 to 9, indicating an acid environment was favorable for Cr (VI) adsorption. As shown in Fig. 6B, the zeta potential of P/Fe$_3$O$_4$@GWBC fell from 27.5 mv to -85.1 mv when pH increased from 2 to 9, and pH$_{zpc}$ was about pH=4.22. As a result, the surface of P/Fe$_3$O$_4$@GWBC was positively charged in pH range of 2-4.22, allowing for the electrostatic attraction of Cr (VI) mainly existing in the form of oxygenate. Contrarily, the negatively charged surface at pH>4.22 repulsed the oxygenate, weakening the Cr (VI) adsorption. Additionally, the competition between oxygenate and OH$^-$ further impaired Cr (VI) adsorption as well.

Kinetic Study

As shown in Fig. 7A, for each starting concentration, the adsorption process had a fast adsorption stage, lasting from the beginning of the test to 240 min, in which about 73.0% and 77.0% of the total Cr (VI) was removed, owing to enough active sites on the surface of the composite for the adsorption, then the adsorption came into a slow stage, which lasted to the end of the test at 2880 min.

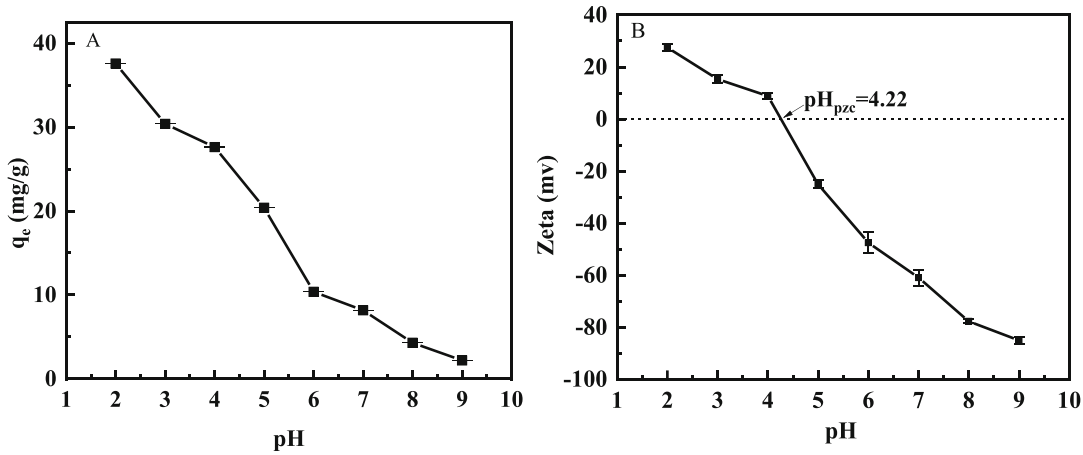Four kinetics models, namely, pseudo-first-order, pseudo-second-order, Elovich models, and intragranular

Fig. 5. The XRD patterns of GWBC (A) and P/Fe$_3$O$_4$@GWBC (B).

Fig. 6. Influence of the initial solution pH on Cr (VI) adsorption by P/Fe$_3$O$_4$@GWBC (A), Zeta potential analysis of P/Fe$_3$O$_4$@GWBC (B) (C$_0$ =50 mg/L , T=298K, t=4 h).

diffusion (Eqs. (1)-(4)) [6, 32] were adopted to explore the adsorption process.

$$\log(q_e - q_t) = \log q_e - \frac{k_1}{2.303}t \qquad (1)$$

$$\frac{t}{q_t} = \frac{t}{q_e} + \frac{1}{k_2 q_e^2} \qquad (2)$$

$$q_t = \frac{1}{\beta}\ln(\alpha\beta) + \frac{1}{\beta}\ln t \qquad (3)$$

$$q_t = k_i t^{1/2} + C \qquad (4)$$

where q$_e$ (mg/g) and q$_t$ (mg/g) were the Cr (VI) uptake at equilibrium and time t, respectively. k$_1$ (1/min) and k$_2$ (g/mg·min) were the pseudo-first-order and pseudo-second-order rate constants, respectively. α (mg/g·min) and β (g/mg) were the initial adsorption rate and the desorption constant, respectively. k$_i$ (mg/g·min$^{1/2}$) was the intragranular diffusion constant, and C was the y-intercept.

Fig. 7B-7D shows the linear fitting using the pseudo-second-order model, the pseudo-first-order model, and the Elovich model, with fitting results presented in Table 2. R^2 of the pseudo-second-order model was higher than those of the pseudo-first-order and the Elovich models; meanwhile, the experimental data of q$_e$ values (37.95 mg/g for C$_0$=50 mg/l and 39.75 mg/g for C$_0$=80 mg/l) were closer to the calculated data from the models, indicating the pseudo-second-order model was more proper than the other two models to describe the adsorption process.

The intragranular diffusion model was used as well to understand the major processes and the rate-limiting step for Cr (VI) adsorption by P/Fe$_3$O$_4$@GWBC [33].

As shown in Fig. 7E, each of the two fitting curves had two linear components, showing that both intro-particle diffusion and surface diffusion took part in the adsorption process. Additionally, as shown in Table 2, ki$_{p1}$ was higher than k$_{ip2}$ for both processes, indicating that the diffusional resistance increased with the quantity of Cr (VI) diffusing into the pores of the adsorbent [34].

Isotherm and Thermal Dynamic Analysis

Langmuir and Freundlich models (Eqs. (5) and (6)) were used to fit the isotherms shown in Fig. 8A, and the results were given in Fig. 8B and 8C.

$$\frac{c_e}{q_e} = \frac{1}{q_m b} + \frac{c_e}{q_m} \qquad (5)$$

$$\log q_e = \log k_f + \frac{1}{n}\log c_e \qquad (6)$$

where C$_e$ (mg/L) was the Cr (VI) concentration at equilibrium, q$_m$ (mg/g) was the theoretical saturated Cr (VI) adsorption calculated from the Langmuir equation, b (L/mg) is the Langmuir constant, k$_f$ and n were the Freundlich model constants, respectively [35].

It can be observed from the R^2 values of the two models listed in Table 3 that the Langmuir model was better at describing Cr (VI) adsorption by the composite.

Table 4 shows the monolayer Cr (VI) adsorption capacity of 11 magnetic adsorbents. P/Fe$_3$O$_4$@GWBC prepared in this study ranked fourth among the composites, indicating it is an effective adsorbent for Cr (VI) removal.

The influence of reaction temperature on Cr (VI) adsorption by P/Fe$_3$O$_4$@GWBC and the feasibility of the process was studied using three thermodynamic parameters, including change in standard free energy (ΔG^0), standard entropy change (ΔS^0), and standard enthalpy change (ΔH^0), which were derived from Eqs. 7 and 8.

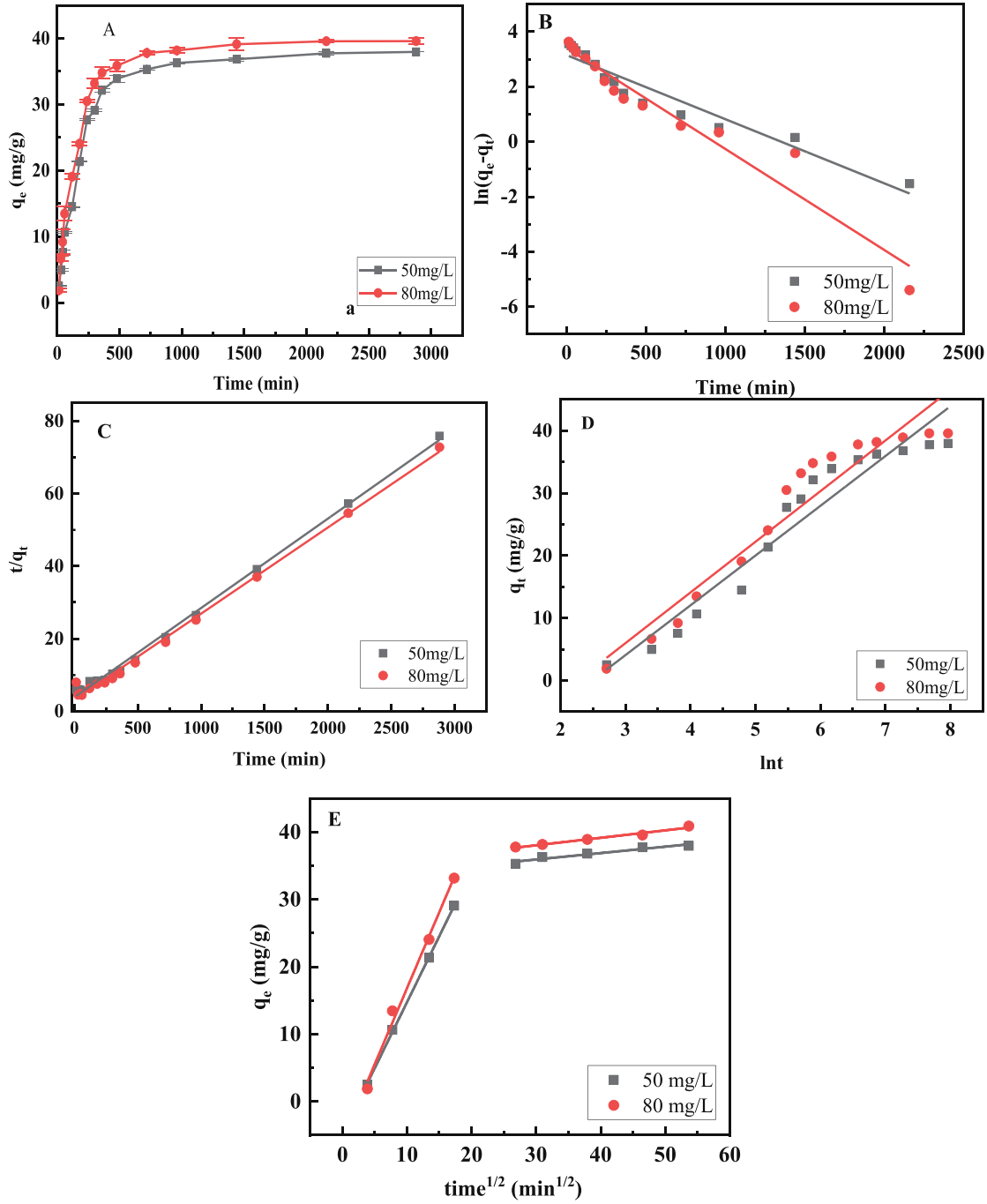$$\Delta G^0 = -RT \ln K_L \qquad (7)$$

Fig. 7. The adsorption kinetics of Cr(VI) by P/Fe$_3$O$_4$@GWBC (A), adsorption kinetics fitted with pseudo-first-order (B), pseudo-second-order (C), Elovich models (D), and intragranular diffusion models (E) (pH=4, T=298K).

$$ln\,K_L = \frac{-\Delta G^0}{RT} = \frac{\Delta S^0}{R} - \frac{\Delta H^0}{RT} \qquad (8)$$

where K_L was a constant from Langmuir isotherm (L/mol); ΔS^0 and ΔH^0 were calculated from the relationship of $ln K_L$ and $1/T$ shown in Fig. 8d, R is the ideal gas constant (8.314 J/(mol·K)), and T is the adsorption temperature (K).

Table 5 shows that the negative values of ΔG^0 for all three adsorption reactions indicated Cr (VI) adsorption by P/Fe$_3$O$_4$@GWBC was spontaneous [46], and the positive values of ΔH^0 and ΔS^0 revealed the adsorption processes had an endothermic nature [2]. Additionally, physical adsorption had a ΔG^0 value and a ΔH^0 value in the range of -20-0 kJ/mol, and 2.1-20.9 kJ/mol in general, respectively [47, 48]. As a result, the ΔG^0 and ΔH^0 values of this study indicated Cr(VI) adsorption by P/Fe$_3$O$_4$@GWBC was mainly physical adsorption.

Influence of Co-Existing Anions

As shown in Fig. 9, all three anions decreased the Cr (VI) adsorption by P/Fe$_3$O$_4$@GWBC in the order of

$PO_4^{3-}>SO_4^{2-}>Cl^-$ due to their competition for the active sites on the surface of $P/Fe_3O_4@GWBC$ with Cr (VI) existing in the form of oxyanions, and increase of the concentration of each anion led to poorer Cr (VI) removal. The presence of the three anions weakened Cr (VI) adsorption more than the solo existence of any individual anion.

Cr (VI) Removal Mechanism

Verifying the Cr (VI) removal mechanism via $P/Fe_3O_4@GWBC$ is crucial as it indicates how the composite will be used in real applications. It was revealed by the experimental results mentioned above that the Cr (VI) removal by $P/Fe_3O_4@GWBC$ was a monolayer chemisorption process with a spontaneous and endothermic nature.

Table 2. Kinetic parameters of Cr (VI) adsorption by $P/Fe_3O_4@GWBC$.

C_0 mg/L	Pseudo-first order			Pseudo-second order			Elovich		
	q_e	k_1	R^2	q_e	k_2	R^2	α	β	R^2
50	23.3470	0.0037	0.9269	40.6000	0.000178	0.9970	86.730	0.126	0.9318
80	30.2330	0.0023	0.9452	42.1050	0.000158	0.9949	77.760	0.123	0.9229

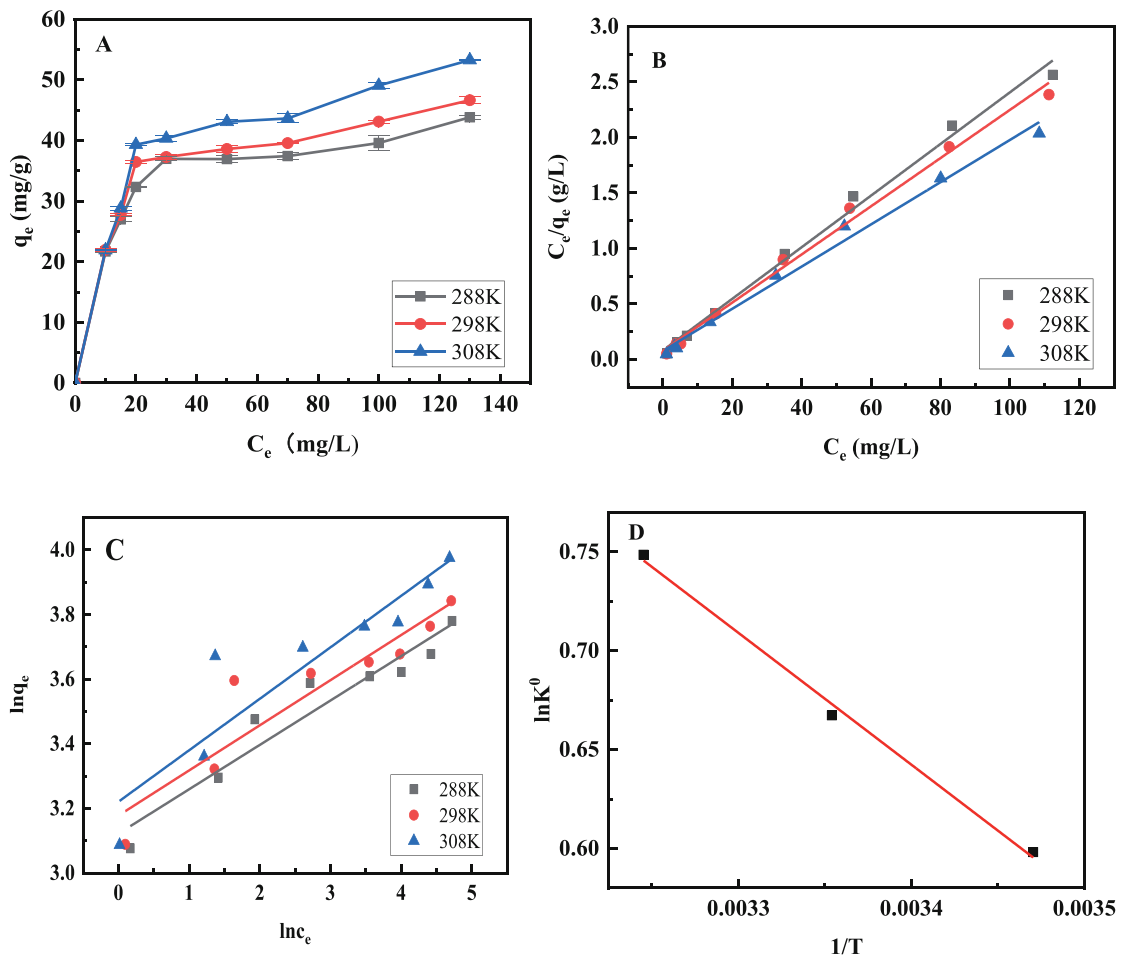| C_0 mg/L	Intra-particle diffusion					
	k_{ip1}	C_1	R_2	k_{ip2}	C_2	R_2
50	1.9602	4.8659	0.9996	0.0953	33.0785	0.9395
80	2.2574	5.7628	0.9918	0.1108	34.7266	0.9758

Fig. 8. The isotherms for Cr (VI) adsorption by $P/Fe_3O_4@GWBC$ under different temperatures (A), the linear fitting by Langmuir model (B), Freundlich model (C), and the relationship between lnK^0 and $1/T$ (D) (pH=4, t=48 h).

Table 3. Parameters of Cr (VI) adsorption by P/Fe$_3$O$_4$@GWBC at different temperatures.

Temperature (K)	Langmuir			Freundlich		
	q_m (mg/g)	K_L (L/mg)	R^2	K_F (mg/g)	n	R^2
288	43.011	0.287	0.993	22.686	7.281	0.926
298	46.083	0.279	0.993	23.992	7.159	0.867
308	52.604	0.250	0.991	25.039	6.278	0.856

Table 4. Comparison of monolayer Cr (VI) adsorption by P/Fe$_3$O$_4$@GWBC with the other reported composites.

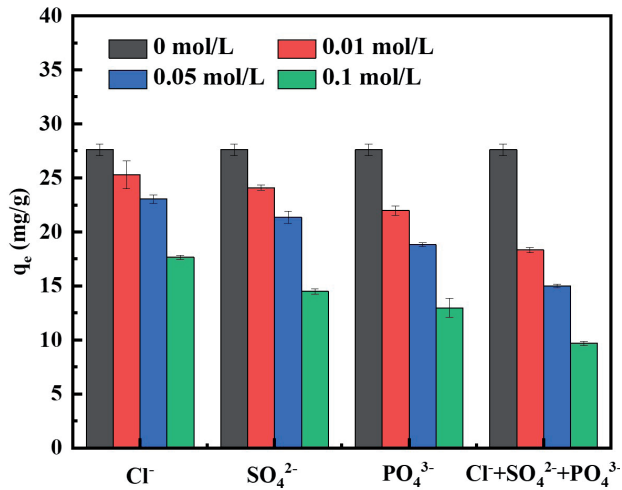| Sample	Reaction conditions		q_{max} (mg/g)	Refer
	pH	Temperature (K)		
Fe-Modified Biochar	2	298	2.78	[36]
	2	308	3.09	
Biochar-based iron oxide composites	-	323	24.37	[37]
G-Fe$_2$O$_3$ nanoparticles	2.5	298	3.3	[38]
Nano-zero-valent iron and sewage sludge biochar	2	298	11.56	[39]
Iron-Zinc Impregnated Biochar Composite	3	298	13.92	[40]
	3	308	21.40	
	3	318	31.22	
Magnetic zeolite/chitosan composite	-	288	21.25	[41]
	-	298	23.76	
	-	308	24.61	
Bagasse magnetic biochar	2	293	29.08	[42]
	2	303	31.37	
	2	313	33.21	
P/Fe$_3$O$_4$@GWBC	4	288	43.01	This study
	4	298	46.08	
	4	308	52.60	
Magnetic porous biochar	-	293	101.01	[43]
	-	303	149.33	
	-	313	202.30	
Fe-Mn Oxide-Modified Biochar	2	303	118.03	[44]
Magnetic biochar ABF-N$_{800}$	2	313	142.86	[45]

The characterizing functional groups on the surface of GWBC (Fig. 10A), P/Fe$_3$O$_4$@GWBC before (Fig. 10B) and after (Fig. 10C) Cr (VI) adsorption were shown in Fig. 10. Compared to GWBC, the new peak at 590 cm^{-1} was attributed to Fe-O-Fe [49], indicating the existence of Fe$_3$O$_4$; meanwhile, the peak at 1384 cm^{-1}, 1636 cm^{-1} and 3180 cm^{-1} was corresponded to the CN stretching of the amide group, CONH in PEI, and N-H stretching of amine group [50-52], indicating the successful loading of Fe$_3$O$_4$ and PEI on GWBC. Additionally, the peak of O-H at 3420 cm^{-1} was amplified. After Cr (VI) adsorption, the peak of NH was reduced obviously, while the peak of -OH and Fe-O-Fe shifted to 3400 cm^{-1} and 580 cm^{-1}, respectively, revealing their involvement in the interaction with Cr (VI).

XPS was used to examine the component of P/Fe$_3$O$_4$@GWBC before and after the adsorption of Cr (VI). The full XPS spectrum is shown in Fig. 11A, and the peaks of Cr2p appeared after adsorption, confirming that Cr (VI) is adsorbed successfully.

Table 5. Thermodynamic parameters of Cr (VI) adsorption by P/Fe$_3$O$_4$@GWBC.

	T (K)	ΔG^0 (kJ/mol)	ΔH^0 (kJ/mol)	ΔS^0 (J·mol^{-1}·K^{-1})
	288K	-1.433		
Cr(VI)	298K	-1.654	5.544	24.266
	308K	-1.918		

Fig. 9. The effect of coexisting ions on adsorption of Cr (VI) by P/Fe$_3$O$_4$@GWBC (T=298K, pH=4, C$_0$=50 mg/L).
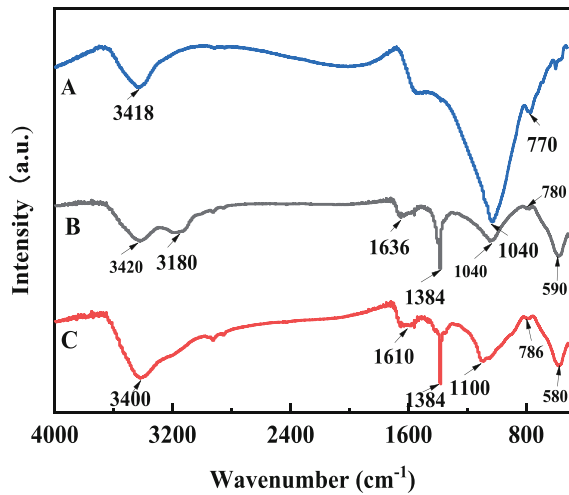
Fig. 10. FTIR spectra of GWBC (A), P/Fe$_3$O$_4$@GWBC before (B) and after (C) Cr (VI) adsorption.

As shown in Fig. 11B,C the peaks at 284.78, 286.19, and 289.46 eV moved to 284.70, 286.18, and 289.01 eV, corresponding to C-C, C-N, and C=N, respectively [53-55]. The peaks of the C1s XPS spectrum were shifted after adsorption (Fig. 11C), indicating the participation of the carbon functional group into the Cr (VI) adsorption. Fig. 11D showed that N 1s spectra contained three peaks at 399.64, 400.3 and 401.43 eV, which corresponded to C-N, -NH$_2$, and -NH^{3+}, respectively [56-58], indicating the presence of Polyethyleneimine. After adsorption,

the peak area of -NH$_2$ decreased from 73.45% to 20.87%; meanwhile, the peak area of -NH$_3^+$ increased from 5.70% to 54.6%, as shown in Fig. 11E. Hence, the results substantiated the amine groups were protonated successfully, which was conducive to attracting Cr (VI) with a negative charge, which can be described by Eqs.9. The peaks at 530.3 and 531.93 eV (Fig. 11F) moved to 530.26 and 531.83 eV (Fig. 11G), corresponding to -OH and C=O respectively (Fig. 11F) [59, 60]. Fig. 11H and Fig. 11I showed the Fe2p high-resolution XPS spectra of P/Fe$_3$O$_4$@GWBC before and after Cr (VI) adsorption. Two peaks at 711.29 and 724.65 eV are attributed to Fe 2p3/2 and Fe 2p1/2 orbitals of Fe^{2+}, respectively [61], and a satellite peak of Fe^{2+} at 720.36 eV before adsorption. Two peaks at 713.89 and 726.02 eV correspond to Fe 2p3/2 and Fe 2p1/2 orbits of Fe^{2+} [62, 63]. After adsorption, the peaks attributed to Fe^{3+} and Fe^{2+} shifted, and a new satellite peak emerged, indicating that the iron-containing group participated in the adsorption of Cr (VI). The peak area of Fe^{3+} increased from 44.25% to 61.70% after adsorption, whereas the peak areas of Fe^{2+} declined from 55.75% to 38.30%. Therefore, as a reductant, the Fe^{2+} in P/Fe$_3$O$_4$@GWBC reduced Cr (VI) into Cr (III), which can be stated by the following Eqs. 10, 11.

$$-NH_2 + H^+ + HCrO_4^- \rightarrow -NH_3^+ \cdots HCrO_4^- \tag{9}$$

$$HCrO_4^- + 7H^+ + 3e^- \rightarrow Cr^{3+} + 4H_2O \tag{10}$$

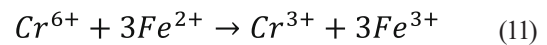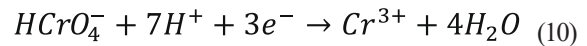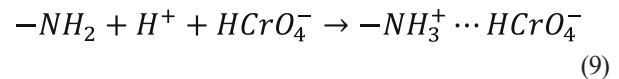$$Cr^{6+} + 3Fe^{2+} \rightarrow Cr^{3+} + 3Fe^{3+} \tag{11}$$

Fig. 11J showed that the peaks at 576.87 eV and 586.71 eV attributed to 2p3/2 and 2p1/2 of Cr (III) [64], and its peak areas increased from 0 to 59.54% after Cr (VI) adsorption. Peaks of 578.3 eV and 588 eV corresponded to 2p3/2 and 2p1/2 of Cr (VI) [65] and accounted for only 40.46% of total Cr, indicating the chelation and reduction of Cr (VI) into Cr (III) with P/Fe$_3$O$_4$@GWBC.

Conclusions

Polyethyleneimine-modified magnetic biochar (P/Fe$_3$O$_4$@GWBC) was prepared in the optimal way determined in this study, and the prepared composite was used to carry out static Cr (VI) removal experiments. The findings showed that Cr (VI) removal by P/Fe$_3$O$_4$@
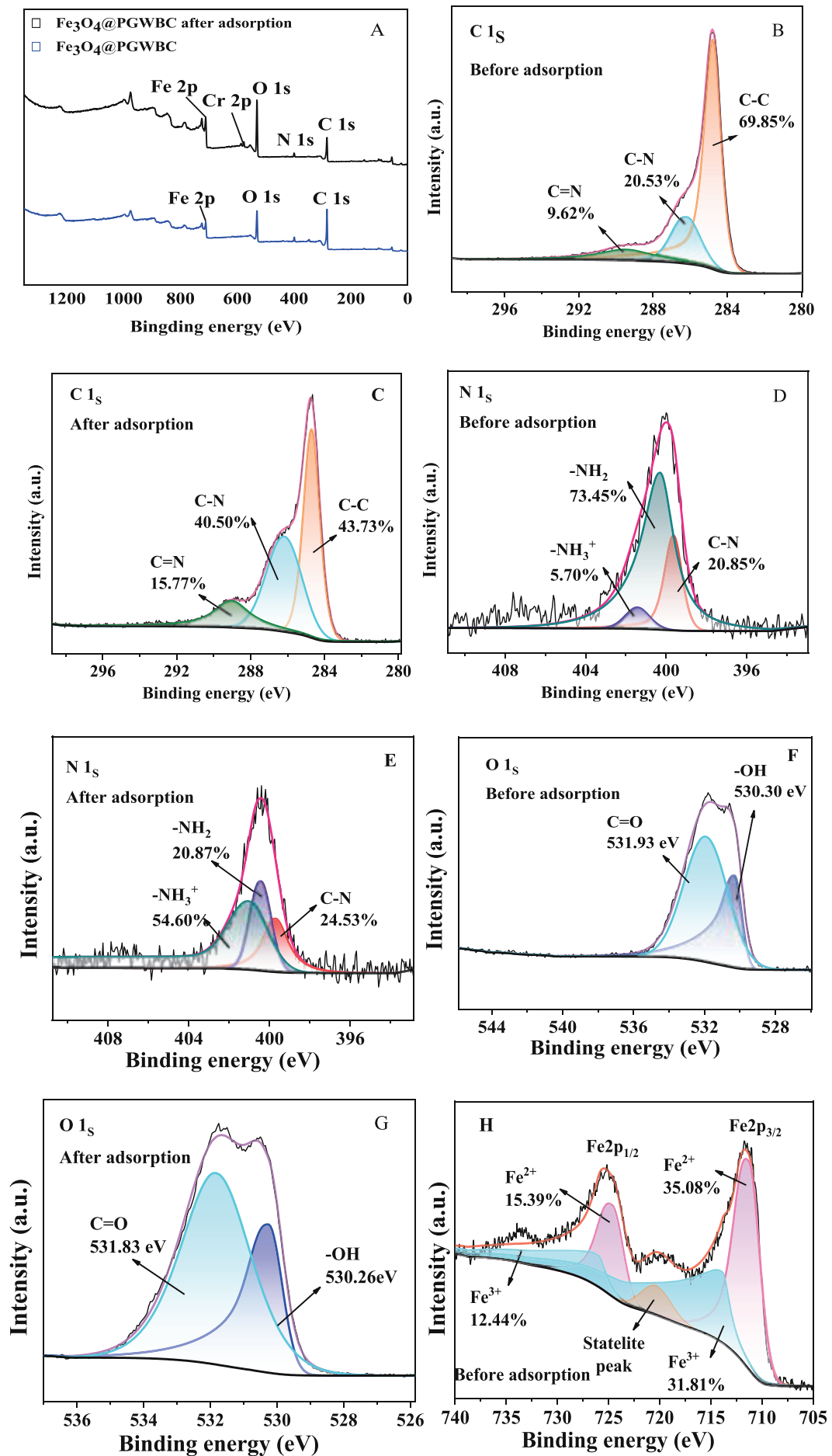
Fig. 11 The full XPS of P/Fe$_3$O$_4$@GWBC before and after Cr (VI) adsorption (A), the detail survey of C1S before (B) after Cr (VI) 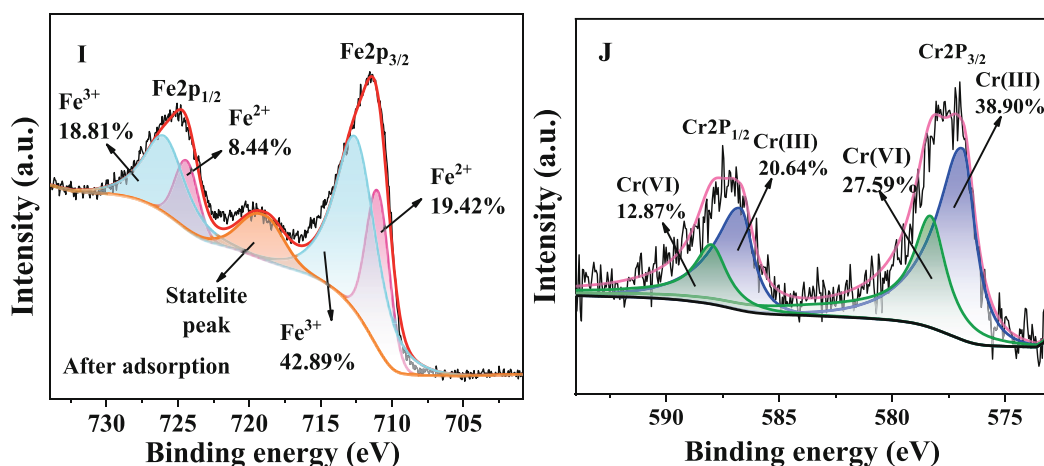adsorption (C), N1S before (D) after Cr (VI) adsorption (E), O1S before (F) after Cr (VI) adsorption (G), F2p before (H) after Cr (VI) adsorption (I), Cr2p after Cr (VI) adsorption (J).

GWBC was pH-dependent, and Cr (VI) adsorption dropped from 37.6 mg/g to 2.2 mg/g as the solution pH rose from 2 to 9. The thermodynamic exploration indicated that the adsorption process was spontaneous and endothermic, and the pseudo-second-order kinetics model described it better than the other two models. Langmuir's model was better than the Freundlich model to fit the experimental data. The greatest theoretical Cr (VI) adsorption capacity obtained from the model was 52.6 mg/g, which was greater than the other 10 types of composites collected from the existing documents. All three anions weakened Cr (VI) removal in the order of $PO_4^{3-}>SO_4^{2-}>Cl^-$, indicating the impact of anions was positively correlated with the charge and concentration. Based on the studies above, electrostatic adsorption, ion exchange, chelation, and Cr (VI) reduction by Fe^{2+} were proposed as the primary processes for Cr (VI) removal.

Conflict of Interest

The authors declare no conflict of interest.

References

1. MIAO S.Y., GUO J.R., DENG Z.M., YU J.X., DAI Y.R. Adsorption and reduction of Cr (VI) in water by iron-based metal-organic frameworks (Fe-MOFs) composite electrospun nanofibrous membranes. Journal of Cleaner Production, **370**, 133566, **2022**.

2. XING X.W., REN X.M., ALHARBI N.S., CHEN C.L. Efficient adsorption and reduction of Cr (VI) from aqueous solution by Santa Barbara Amorphous-15 (SBA-15) supported Fe/Ni bimetallic nanoparticles. Journal of Colloid and Interface Science, **629** (A), 744, **2023**.

3. CHANG J.J., ZHANG J., WANG H., BAI Y.F., LIU Y., BI Y.Z., ZHANG H.Z., CHEN H.H., BARNIE S., XIE H.J. Cr (VI) adsorption and reduction by magnetite-humic acid adsorption complexes under mildly acidic conditions: Synergistic/antagonistic mechanism and multi-step reaction model. Chemical Engineering Journal, **451** (B), 138648, **2023**.

4. TATTIBAYEVA Z., TAZHIBAYEVA S., KUJAWSKI W., ZAYADAN B., MUSABEKOV K. Peculiarities of adsorption of Cr (VI) ions on the surface of Chlorella vulgaris ZBS1 algae cells. Heliyon, **8** (9), e10468, **2022**.

5. SHARMA P., PRAKASH J., PALAI T., KAUSHAI R. Surface functionalization of bamboo leave mediated synthesized SiO$_2$ nanoparticles: Study of adsorption mechanism, isotherms and enhanced adsorption capacity for removal of Cr (VI) from aqueous solution. Environmental Research, **214** (1), 113761, **2022**.

6. QASEM K.M.A., KHAN S., CHINNAM S., SALEH H.A.M., I M., ZEESHAN M., MANEA Y.K., SHAHID M. Sustainable fabrication of Co-MOF@CNT nano-composite for efficient adsorption and removal of organic dyes and selective sensing of Cr (VI) in aqueous phase. Materials Chemistry and Physics, **291**, 126748, **2022**.

7. TIE J.X., LI W.P., LIU H.Y., HUANG K., MI X., WEI M.H., HOU L.J. Efficient adsorption and reduction of Cr (VI) by a novel polyaniline modified magnetic iron-based waterworks sludge from aqueous solution. Chemical Engineering Journal, **451** (3), 137673, **2023**.

8. YANG W.L., LEI G., QUAN S.J., ZHANG L.F., WANG B.T., HU H., LI L.L., MA H., YIN C.H., FENG F., JING Y.Y. The Removal of Cr (VI) from Aqueous Solutions with Corn Stalk Biochar. International Journal of Environment, **19** (21), 14188, **2022**.

9. BENIS K.Z., MINAEI S., SOLTAN J., MCPHEDRAN K.N. Adsorption of lincomycin on microwave activated biochar: Batch and dynamic adsorption. Chemical

Engineering Research & Design, **187**, 140, **2022**.

10. IBERAHIM N., SETHUPATHI S., BASHIR M.J.K., KANTHASAMY R., AHMAD T. Evaluation of oil palm fiber biochar and activated biochar for sulphur dioxide adsorption. Science of the Total Environment, **805**, 150421, **2022**.

11. LIU T.Q., LAWLUVY Y., SHI Y., HE Y., ZHANG Y.J., YAP P.S. Adsorption of cadmium and lead from aqueous solution using modified biochar: A review. Journal of Environmental Chemical Engineering, **10** (1), 106502, **2022**.

12. BAYRAM O., ÖZKAN U., SAHIN H.T., GÖDE F. Malachite green (cationic dye) removal with modified *pinus brutia* biochar. Internalization Journal of Phytoremediation, **26** (3), 416, **2024**.

13. WANG J., QIAN W., HE Y., XIONG, Y., SONG P., WANG R.M. Reutilization of discarded biomass for preparing functional polymer materials. Waste Management, **65**, 11, **2017**.

14. MUJTABA G., HAYAT R., HUSSAIN Q., AHMED M. Physio-chemical characterization of biochar, compost and co-composted biochar derived from green waste. Sustainability, **13** (9), 4628, **2021**.

15. THINES K.R., ABDULLAH E.C., MUBARAK N.M., RUTHIRAAN M. Synthesis of magnetic biochar from agricultural waste biomass to enhancing route for waste water and polymer application: a review. Renewable and Sustainable Energy Reviews, **67**, 257, **2017**.

16. DAI Y., SUN Q., WANG W., LU L., LIU M., LI J., YANG S., SUN Y., ZHANG K., XU J., ZHENG W. Utilizations of agricultural waste as adsorbent for the removal of contaminants: A review. Chemosphere, **211**, 235, **2018**.

17. SOHRABI H., AMERI E. Adsorption equilibrium, kinetics, and thermodynamics assessment of the removal of the reactive red 141 dye using sesame waste. Desalination and Water Treatment, **57** (38), 18087, **2016**.

18. CHERADHI E., AMERI E., MOHEB A. Adsorption of cadmium ions from aqueous solutions using sesame as a low-cost biosorbent: kinetics and equilibrium studies. International Journal of Environmental Science and Technology, **12**, 2579, **2015**.

19. AMERI E., AZIZI, H.Z., MOHEB A. Wheat straw as Low Cost Adsorbent for Pb (II) Removal: Adsorption and Equilibrium. The 8th International Chemical Engineering Congress & Exhibition (IChEC 2014) Kish Iran, **2014**.

20. CHERADHI E., AMERI E., MOHEB A. Continuous biosorption of Cd (II) ions from aqueous solutions by sesame waste: thermodynamics and fixed-bed column studies. Desalination and Water Treatment, **57** (15), 6936, **2016**.

21. JAHANGIRI A., AMERI E. Experimental investigation on Cadmium ions removal from aqueous solutions by modified wheat straw biosorbent. Journal of Environmental Science and Technology, **19** (1), 31, **2017.**

22. VENKATRAMAN Y., ARUNKUMAR P., KUMAR N.S., OSMAN A.I., MUTHIAH M., AL-FATESH A.S., KODURU J.R. Exploring Modified Rice Straw Biochar as a Sustainable Solution for Simultaneous Cr (VI) and Pb(II) Removal from Wastewater: Characterization, Mechanism Insights, and Application Feasibility, ACS Omega, **8** (41), 38130, **2023**.

23. DU Z.C., YANG M., YANG Y.F., ZHANG X.L., CHEN H.H., NGO H.H., LIU Q. Sulfur-Modified Biochar Efficiently Removes Cr (VI) from Water by Sorption and Reduction. Environmental Engineering Science, **40** (9), 362, **2023**.

24. LIU Y.B., LIU F.Q., DING N., SHEN C.S., LI F., DONG L.M., HUANG M.H., YANG B., WANG Z.W., SAND W. Boosting Cr (VI) detoxification and sequestration efficiency with carbon nanotube electrochemical filter functionalized with nanoscale polyaniline: performance and mechanism. Science of the Total Environment, **695**, 133926, **2019**.

25. MAO W., ZHANG Y., LUO J.E., CHEN L.T., GUAN Y.T. Novel co-polymerization of polypyrrole/polyaniline on ferrate modified biochar composites for the efficient adsorption of hexavalent chromium in water. Chemosphere, **303** (3), 135254, **2022**.

26. KERMANNEZHAD J., TORABIPOODEH H., GHANBARI-ADIVI E., SHAHINEZHAD B. Removal of pollutants from aqueous solution with magnetic biochar: a mini review. Particulate Science and Technology, **42** (3), 361, **2024**.

27. LIN J.F., WANG C.H., LEE M.Z. Linear birefringence and dichroism measurement in oil-based Fe_3O_4 magnetic nanoparticles. Journal of Magnetism and Magnetic Materials, **332**, 192, **2018**.

28. JUANG R.S., SU C.J., WU M.C., LU H.C., WANG S.F., SUN A.C. Fabrication of magnetic Fe_3O_4 nanoparticles with unidirectional extension pattern by a facile and eco-friendly microwave-assisted solvothermal method. Journal of Nanoscience and Nanotechnology, **19** (12), 7645, **2019**.

29. MAJID F., BASHIR M., BIBI I., AYUB M., KHAN B.S., SOMAILY H.H., AL-MIJALLI S.H., NAZIR A., IQBAL S., IQBAL M. Green synthesis of magnetic Fe_3O_4 nanoflakes using vegetables extracts and their magnetic, structural and antibacterial properties evaluation. Zeitschrift Für Physikalische Chemie, **237** (9), 1345, **2023**.

30. LIANG Y.X., JIANG L., XU S.T., JU W.T., TAO Z., YANG Y.M., PENG X.L., WEI G.W. Synthesis and characterization of Fe_3O_4 nanoparticles prepared by solvothermal method. Journal of Materials Engineering Performance, **6**, 1, **2023**.

31. YULIANA F., SUNARYONO S., ZULAIKAH S. The effect of PVP on structural of $Fe_3O_4@$ TiO_2 nanocomposite. AIP Conference Proceedings, **2858** (1), 060013, **2023**.

32. HIDAYER A.R.P., WIDYANTO A.R., ZULFA L.L., ASRANUDIN A., SUGIARSO D., PUTRO H.S., PURNOMO A.S., PRASETYOKO D., PRIYANGGA A., ATMAJA L., ASIKIN-MIJAN N., ADZAHAR N.A., EDIATI R. Mechanism adsorption-reduction into the incorporation of microbial fuel cell-metal organic framework and overview of hydrodynamics effects for enhanced reduction of Cr (VI). Journal of Water Process Engineering, **49**, 103095, **2022**.

33. ZHENG Z.H., ZHAO B.L., GUO Y.P., GUO Y.J., PAK T., LI G.T. Preparation of mesoporous batatas biochar via soft-template method for high efficiency removal of tetracycline. Science of the Total Environment, **787**, 147397, **2021**.

34. TIE J.X., SANG S., SHANG Z.Y., LI Y.Q., XU Z.T., LIAN M.L., DU C.B. Preparation of Al-loaded magnetic Chinese medicine residue-derived biochar and application of it in fluoride removal. Industrial Crops and Products, **184**, 115037, **2022**.

35. SHI S.Q., YANG J.K., LIANG S. Enhanced Cr (VI) removal from acidic solutions using biochar modified by $Fe_3O_4@SiO_2$-NH_2 particles. Science of the Total Environment, **628-629**, 499, **2018**.

36. PAN R., BU J.P., REN G.Y., ZHANG Z.H., LI K.X., DING A.F. Mechanism of removal of hexavalent chromium

from aqueous Solution by Fe-modified biochar and its application. Applied Sciences, **12**, 1238, **2022**.

37. DONG F.X., YAN L., ZHOU X.H., HUANG S.T., LIANG J.Y., ZHANG W.X., GUO Z.W., GUO P.R., QIAN W., KONG L.J., CHU W., DIAO Z.H. Simultaneous adsorption of Cr (VI) and phenol by biochar-based iron oxide composites in water: Performance, kinetics and mechanism. Journal of Hazardous Materials, **416**, 125930, **2021**.

38. HU J., CHEN G.H., LO I.M.C. Removal and recovery of Cr (VI) from wastewater by maghemite nanoparticles. Water Research, **39** (18), 4528, **2005**.

39. LIU L.H., LIU X., WANG D.Q., LIN H., HUANG L. Removal and reduction of Cr(VI) in simulated wastewater using magnetic biochar prepared by co-pyrolysis of nano-zero-valent iron and sewage sludge. Journal of Cleaner Production, **257**, 120562, **2020**.

40. QHUBU M.C., METHULA B., XABA T., MOYO M., PAKADE V.E. Iron-Zinc impregnated biochar composite as a promising adsorbent for toxic hexavalent chromium remediation: kinetics, isotherms and thermodynamic. Chemistry Africa, **5**, 1797, **2022**.

41. LIU X.Q., LIU Y., ZHANG T.A. Preparation of magnetic zeolite/chitosan composite using silane as modifier for adsorption of Cr (VI) from aqueous solutions. Journal of Vinyl and Additive Technology, **27** (3), 640, **2021**.

42. LIANG M.N., DING Y.M., ZHANG Q., WANG D.Q., LI H.H., LU L. Removal of aqueous Cr (VI) by magnetic biochar derived from bagasse. Scientific Reports, **10**, 21473, **2020**.

43. QU J.H., WANG S.Q., JIN L.Y., LIU Y., JIANG Z., TAO Y., HUANG J.J., ZHANG Y. Magnetic porous biochar with high specific surface area derived from microwave-assisted hydrothermal and pyrolysis treatments of water hyacinth for Cr(VI) and tetracycline adsorption from water. Bioresource Technology, **340**, 125692, **2021**.

44. ZHU Y.Y., DAI W.C., DENG K., PAN T., GUAN Z.J. Efficient removal of Cr (VI) from aqueous solution by Fe-Mn oxide-Modified biochar. Water Air and Soil Pollution, **231**, 61, **2020**.

45. MIAN M.M., LIU G.J., YOUSAF B., FU B., ULLAH H., ALI M.U., ABBAS Q., MUNIR M.A.M., LIU R.J. Simultaneous functionalization and magnetization of biochar via NH_3 ambiance pyrolysis for efficient removal of Cr (VI). Chemosphere, **208**, 712, **2018**.

46. TAN X., ZHANG Y.J., LIU M., CAO J.M., DUAN G.L., CUI J., LIN A.J. Ultrasonic-assisted preparation of interlaced layered hydrotalcite (U–Fe/Al-LDH) for high-efficiency removal of Cr (VI): Enhancing adsorption-coupled reduction capacity and stability. Chemosphere, **308** (3), 136472, **2022**.

47. LIU Y. Is the free energy change of adsorption correctly calculated? Journal of Chemical Engineering, **54** (7)**,** 1981, **2009**.

48. O'CONNELL D.W., BIRKINSHAW C., O'DWYER T.F. Heavy metal adsorbents prepared from he modification of cellulose: a review. Bioresoure Technology, **99** (15), 6709 **2008**.

49. NAZARI S., MEHRI A., HASSANNIA A.S. Fe_3O_4-modified graphene oxide as a sorbent for sequential magnetic solid phase extraction and dispersive liquid phase microextraction of thallium. Microchimica Acta, **184**, 3239, **2017**.

50. THOMBARE N., MAHTO A., SINGH D., CHOWDHURY A.R., ANSARI M.F. Comparative FTIR characterization of various natural gums: a criterion for their identification.

Journal of Polymers and the Environment, **31** (8), 3372, **2023**.

51. EID M.E.S. Polyethylenimine-functionalized magnetic amorphous carbon fabricated from oil palm leaves as a novel adsorbent for Hg(II) from aqueous solutions. Egyptian Journal of Petroleum, **27** (4), 1051, **2018**.

52. DANI M.S.H., VENKATESHWARAH N. Role of surface functionalized crystalline nano-silica on mechanical, fatigue and drop load impact damage behaviour of effective stacking sequenced E-glass fibre-reinforced epoxy resin composite. Silicon, **13**, 757, **2021**.

53. BIAN Y., BIAN Z.Y., ZHANG J.X., DING A.Z., LIU S.L., ZHENG L., WANG H. Adsorption of cadmium ions from aqueous solutions by activated carbon with oxygen-containing functional groups. Chinese Journal of Chemical Engineering, **23** (10), 1705, **2015**.

54. CHAUDHURI H., LIN X.Y., YUN Y.S. Graphene oxide-based dendritic adsorbent for the excellent capturing of platinum group elements. Journal of Hazardous Materials, **451**, 131206, **2023**.

55. MING F.L., HOU J.Z., HOU C.J., YANG M., WANG X.F., LI J.W., HUO D.Q., HE Q. One-step synthesized fluorescent nitrogen doped carbon dots from thymidine for Cr (VI) detection in water. Spectrochimica Acta Part A: Molecular and Biomolecular Spectroscopy, **222**, 117165, **2019**.

56. DANYILDIZ Z., UZUN D., CALAM T.T., HASDEMIR E. A voltammetric sensor based onglassy carbon electrode modified with 1H-1,2,4-triazole-3-thiol coating for rapid determination of trace lead ions in acetate buffer solution. Journal of Electroanalytical Chemistry, **805** (15), 177, **2017**.

57. WANG D., JONES F.R. Surface analytical study of the interaction between y-amino propyl triethoxysilane and E-glass surface Part II X-ray photoelectron spectroscopy. Journal of Materials Science, **28**, 2481, **1993**.

58. ZHU X.Y., BAI R.B., WEE K.O., LIU C.K., TANG S.L. Membrane surfaces immobilized with ionic or reduced silver and their anti-biofouling performances. Journal of Membrane Science, **363** (1-2), 278, **2010**.

59. ABDETA A.B., WU Q.H., KUO D.H., LI P., HUANG T., ZHANG J.B. MOSISA M.T., LIN J.G., CHEN X.Y. Mo(S,O)/(Ce,Mo)(S,O) sulfo-oxide with heterovalent metal states for efficient visible-light-driven hydrogen evolution and pollutant reduction via in-situ generated protons. International Journal of Hydrogen Energy, **48** (29), 10841, **2023**.

60. QIAN X.Y., LI F., JIN L.N. MOF drived MnO/N-C/CNT composite and its modified separator foradvanced Li-S battery. Microporous and Mesoporous Materials, **329**, 111558, **2022**.

61. MA K.X., ZHANG M.X., MIAO S.C., GU X.Y., LI N., CUI S.H., YANG J. Magnetic solid-phase extraction of pyrethroid pesticides in environmental water samples with $CoFe_2O_4$-embedded porous graphitic carbon nanocomposites. Journal of Separation Science, **41** (17), 3441, **2018**.

62. MALEKI M.H., SHIRANI M.A., DINARI M. Facile synthesis of green and efficient copper-based magnetically recoverable nanocatalyst for the reduction of nitrophenol derivatives. Journal of Molecular Liquids, **365**, 120189, **2022**.

63. APIWON-NAGARM K., PONGWAN P., INCEESUNGVORN B., PHANICHPHANT S., WETCHAKUN K., WETCHAKUN P. Photocatalytic activities of Fe-Cu/TiO₂ on the mineralization of oxalic

acid and formic acid under visible light irradiation. Powder Technology, **266**, 447, **2014**.

64. LI Y., WEI G.L., ZHANG C.H., LIANG X.L., CHU W., HE H.P., STUCKI J.W., MA L.Y., LIN X.J., ZHU J.X. Remarkable effect of Co substitution in magnetite on the reduction remaval of Cr (VI) coupled with aqueous Fe (II): Improvement mechanism and Cr fate. Science of the Total Environment, **656**, 400, **2019**.

65. WANG C., XIONG C., HE Y.L., YANG C., LI X.T., ZHENG J.Z., WANG S.X. Facile Preparation of Magnetic Zr-MOF for Pb(II) and Cr (VI) from Water: Adsorption Characteristics and Mechanisms. Chemical Engineering Journal, **415**, 128923, **2021**.